Engineering Structures 219 (2020) 110537

Contents lists available at ScienceDirect

Engineering Structures

journal homepage: www.elsevier.com/locate/engstruct

Two-way bending experimental response of URM walls subjected to combined horizontal and vertical seismic excitation

S. Sharma[a], U. Tomassetti[b], L. Grottoli[c], F. Graziotti[c,d,*]

[a] UME School, Istituto Universitario di Studi Superiori - IUSS, Piazza della Vittoria 15, 27100 Pavia, Italy
[b] Willis Re, Willis Towers Watson, 51 Lime Street, London EC3M 7DQ, United Kingdom
[c] European Centre for Training and Research in Earthquake Engineering – EUCENTRE, Via Ferrata 1, 27100 Pavia, Italy
[d] Dept. of Civil Engineering and Architecture – DICAr, University of Pavia, Via Ferrata 3, 27100 Pavia, Italy

ARTICLE INFO

Keywords:
Out-of-plane
Two-way bending
Incremental dynamic tests
Unreinforced masonry
Vertical excitation

ABSTRACT

This paper presents the results of incremental dynamic tests on full-scale unreinforced masonry (URM) walls constructed with an intentionally weakened mortar under two-way bending excitation in the out-of-plane (OOP) direction. A specimen was also subjected to simultaneous vertical and horizontal excitation. Walls were also tested in boundary conditions that have not been previously reported in the literature. Emphasis was placed on the development and interpretation of a characterisation test to estimate the torsional shear strength of bed-joints, a parameter of prime importance in the OOP two-way bending behaviour of URM walls. Analytical formulation to estimate the initial stiffness of walls based on the theory of plates is then proposed and validated. Being the first experimental campaign to address the dynamic OOP two-way bending response of full-scale URM wall panels provided the opportunity to propose simple yet mechanically rational methodologies with which both the peak force resistance as well as the displacement at which such resistance is attained can be easily estimated.

1. Introduction

The vast majority of the studies addressing the significant risk posed by unreinforced masonry (URM) buildings under seismic action have focused on the primary load transfer path of seismic forces in a URM structure i.e. the in-plane direction of walls [1–4]. In reality, the seismic resistance of URM structures resulting from following of this load path is often not completely realised due to the occurrence of out-of-plane (OOP) failure mechanisms. Such failures have also been widely documented in numerous post-earthquake surveys [5–9]. Hence, for the full seismic capacity of a URM structure to be realised, OOP failures have to be prevented first. However, in contrast to studies on the behaviour of URM in the in-plane direction, research on the behaviour of URM in the OOP direction is comparatively limited. While some work has been carried out on one-way spanning URM panels (with no lateral edges supported) [10–14], experimental studies on the behaviour of two-way spanning URM panels (with at least one lateral edge supported) is limited to inclined table [15] and air bag tests [16,17] on half-scale masonry walls, cyclic tests of full-scale mortared [18,19] and dynamic tests on half-scale mortared walls [20]. Additionally, in-situ quasi-static airbag tests were also performed by Walsh *et al.* [21] on walls in an existing building. In fact, what had been missing entirely from literature are dynamic tests generating loading conditions as that in a real earthquake on full scale URM walls until recent work by the same authors in Graziotti *et al.* [22] and Tomassetti *et al.* [23].

This paper presents the outcomes of an experimental campaign envisaged to thoroughly understand the behaviour of full-scale unreinforced masonry walls (URM) under dynamic two-way bending excitation. The experimental tests reported here were performed as a part of an ongoing project at EUCENTRE, Pavia [24] to assess the vulnerability of unreinforced buildings currently subjected to induced seismicity due to natural gas extraction in the Groningen province, the Netherlands [25,26]. Within the same project, progress in the domain of OOP response of URM has already been made in the form of dynamic tests of URM panels in a one-way bending condition [11] as well as the development and calibration of numerical models capturing their behaviour observed in those tests [27]. Four single leaf walls and one double leaf cavity wall were incrementally dynamically tested until collapse or a near collapse scenario in Graziotti *et al.* [22]. One of these specimens was restrained on all four sides with the top edge loaded with pre-compression. All others walls were restrained on three sides and had their top edge free and unloaded, with one of these specimens

* Corresponding author at: Dept. of Civil Engineering and Architecture – DICAr, University of Pavia, Via Ferrata 3, 27100 Pavia, Italy.
E-mail address: francesco.graziotti@unipv.it (F. Graziotti).

https://doi.org/10.1016/j.engstruct.2020.110537
Received 7 November 2019; Received in revised form 19 February 2020; Accepted 13 March 2020
Available online 01 July 2020

also possessing a large opening. The majority of the specimens tested in Graziotti *et al.* [22] corresponded to masonry which exhibits failure under pure horizontal bending by the splitting of units.

Of the four full-scale specimens presented in this article, two specimens had both vertical edges and the bottom edge restrained while the top edge was kept unloaded and free. Of these, one was subjected to biaxial seismic excitation: simultaneous dynamic horizontal OOP and vertical input, a test that has not been performed and reported in existing literature yet. The other two specimens corresponded to a boundary condition which was not tested yet in [22]: both having only one vertical and the bottom edge restrained but corresponding to different lengths and aspect ratios. For each full-scale specimen, the observed progression of structural damage through the testing sequence, force-displacement hysteresis curves as well as change in the first natural mode of vibration of the walls throughout the testing sequence was monitored.

URM, especially while assessing or designing against OOP loading can be broadly distinguished into two distinct typologies based on their response under pure-horizontal bending. The first typology can be classified as "Weak Unit-Strong Joint" (WU-SJ) and exhibits a vertical crack passing through the brick units and head joints under pure horizontal bending. The second typology, i.e. "Strong Unit-Weak Joint" (SU-WJ), exhibits a stepped crack passing through head joints and half a bed joint under pure horizontal bending. Bending resistance being derived from the flexural strength of units and the torsional shear strength of bed-joints in the first and second typology respectively. Specimens tested in the current work were constructed in masonry that corresponded to a much weaker mortar with respect to Graziotti *et al.* [22]. This was done in order to bring about a change in the failure mode of the tested masonry under pure horizontal bending from a WU-SJ to a SU-WJ typology. To achieve this, design of the masonry to be used for constructing the specimens was done using state-of-the art analytical equations present in literature [28,29]. The adopted design methodology is presented in the first section of this paper. Quasi-static experiments on horizontal URM beams performed to experimentally validate the adopted design methodology highlighted the importance of further understanding of the torsional shear strength of unreinforced masonry and development of a novel characterization test addressing the same proposed in [22].

Virtual-work-method-based formulation for estimating the peak OOP two-way bending force resistance of URM walls which had been explained in detail while presenting the results in Graziotti *et al.* [22] were again applied and validated for the tested specimens. Analytical formulation based on the theory of plates, is presented and verified to provide a reasonable estimate of wall stiffness at the attainment of peak strength.

2. Design of the experimental campaign

A majority of the specimens tested in Graziotti *et al.* [22] (three of the single leaf specimens and one of the leaves of the cavity wall) were constructed in masonry possessing material characteristics which corresponded to a WU-SJ typology. Such specimens exhibited a considerably brittle response under two-way bending excitation, especially in configurations in which the top edge was left free and unloaded: failure was controlled primarily by the splitting of masonry units. However, one of the primary objectives of the entire experimental campaign was to create a reliable database of experimental data with which numerical models for estimating the OOP response of URM can be well calibrated. Keeping this in mind, it was envisaged to create a set of walls corresponding to a SU-WJ typology by weakening the mortar while using the same Calcium Silicate (CS) units as [22].

2.1. Adopted design methodology

State-of-the-art expressions for calculating the moment capacities associated under horizontal bending with WU-SJ and the SU-WJ URM configurations were used to design the masonry of the walls. These models which were initially proposed by Willis [29] and successively revised by Griffith and Vaculik [18] calculate M_h, i.e. the unit crack length capacity in terms of moment due to horizontal bending as per Eqs. (1) and (2) respectively:

$$M_h = \frac{1}{2(h_u + t_j)}\left[(f_{ut} - \nu\cdot\sigma)\cdot h_u \frac{t_u^2}{6}\right] \quad \text{WU} - \text{SJ} \ \text{(line failure)} \tag{1}$$

$$M_h = \frac{1}{h_u + t_j}[\tau_{tor}\cdot k_b\cdot 0.5\cdot(l_u + t_j)\cdot t_u^2] \quad \text{SU} - \text{WJ} \ \text{(stepped failure)} \tag{2}$$

In Eqs. (1) and (2), the length, height and thickness of a brick are represented by l_u, h_u and t_u respectively; the thickness of a joint is represented by t_j; f_{mt} is the tensile strength of masonry perpendicular to bed-joints; f_{ut} the tensile strength of a masonry units, σ is the vertical stress acting on the wall at its mid-height and ν is the Poisson's ratio of masonry. τ_{tor} here denotes the shear strength of a masonry bed-joint under torsion and k_b is a numerical factor used to compute shear stress due to torsion acting on a rectangular shaft while assuming a linear elastic distribution of stress, adopted as 0.208 [30].

While the value of f_{ut} can be easily calculated by standard characterisation tests [31], there currently exists no standardized procedure to estimate the torsional shear strength of masonry bed joints. Only two equations can be found in literature to estimate the value τ_{tor}, the first one being a dimensionally inconsistent empirical equation present in the Australian Masonry Structures Code, AS 3700 [32] which estimates the strength of masonry bed-joints under torsional shear as $\tau_{tor} = 2.25(f_{mt})^{1/2}$ where f_{mt} is the tensile strength (in MPa) in a direction perpendicular to bed-joints and can be evaluated from standardized characterization tests [33]. The second equation, again developed by Willis [29] is dimensionally consistent and was developed based on torsional shear experiments on masonry bed-joints and revised on the basis of a review of then existing in-plane behaviour of masonry estimates $\tau_{tor} = 0.9\sigma + 1.6f_{mt}$. This formula was used in Eq. (3) to estimate the value of τ_{tor} (and consequently f_{mt} in Eq. (4)) for which the torsional shear strength of masonry bed-joints would be low enough to result in "SU-WJ" typology URM i.e. by equating Eqs. (1) and (2):

$$\tau_{tor} = 1.6\cdot f_{mt} + 0.9\cdot\sigma = \frac{h_u}{6\cdot k_b\cdot(l_u + t_j)}[(f_{ut} - \nu\cdot\sigma)] \tag{3}$$

$$f_{mt} = \frac{h_u}{9.6\cdot k_b\cdot(l_u + t_j)}[(f_{ut} - \nu\cdot\sigma)] - 0.5625\cdot\sigma = 0.41 \ \text{MPa} \tag{4}$$

As already mentioned, the intention was to design masonry corresponding to a SU-WJ configuration by weakening the masonry joint and

Table 1
Comparison of mechanical properties of masonry in the current study compared to Graziotti *et al.* [22]

			f_m	E	f_{mt}	f_c	f_t	f_u	f_{ut}	f_{vo}	μ
Graziotti *et al.* [22]	*Mean*	[MPa]	9.74	4784	0.95	8.49	2.72	15.31	2.61	0.81	0.46
	C.o.V.	[%]	7.8	18.0	18.2	32.9	31.3	6.1	14.5	–	–
Current study	*Mean*	[MPa]	7.29	5943	0.22	1.39	0.31	15.31	2.61	0.13	0.55
	C.o.V.	[%]	11.75	9.6	51.1	31.9	50.3	6.1	14.5	–	–

keeping the masonry units the same as [22]. Four out of the five specimens tested in [22] were constructed in CS units measuring 212x102x71 mm ($l_u \times t_u \times h_u$) possessing a flexural tensile strength (f_{ut}) of 2.61 MPa (Table 1) and with mortar joints having a thickness of 10 mm (t_j). Using these parameters, Eq. (4) predicts a f_{mt} value of 0.41 MPa to be the limiting value of flexural tensile strength of masonry below which masonry corresponds to a WU-SJ configuration for these specific CS units and joint thickness. This value of f_{mt} corresponds to a value of $\tau_{tor} = 1.6 \cdot (0.41) = 0.65$ MPa under zero vertical pre-compression as per the torsional shear strength relationship proposed by Willis [29]. It is important to note here that the CS masonry in [22] corresponded to a f_{mt} value of 0.95 MPa which is well above this limit predicted by Eq. (5) and had corresponded to a "WU-SJ" configuration.

With these calculations, the pre-mixed mortar used for constructing the CS masonry in [22] was mixed with 50% sand by volume in an attempt to weaken the mortar and subsequently f_{mt} to a value lower than 0.41 MPa. This attempt was successful as the value of f_{mt} dropped down to a value of 0.22 MPa from 0.95 MPa and is well below the limit calculated using Eq. (4). Characterization tests were also performed to evaluate other parameters, namely: strength of masonry in compression (f_m), modulus of elasticity (secant modulus between 10% f_m-33% f_m) in compression (E), and tension (f_{mt}) perpendicular to bed-joints, strength under compression (f_c) and flexure (f_t) of mortar, strength under compression (f_u) and flexure (f_{ut}) of units and the cohesion and friction coefficient of masonry bed joints under direct (f_{v0} and μ) shear [34–36,31,37]. A summary of these mechanical properties for CS masonry in [22] as well as the current study has been provided in Table 1. It can be observed that all material parameters (other than brick tensile and compressive strength which remained equal as the same units were used) consistently decreased.

In order to experimentally verify the validity of the limit on f_{mt} for the transition between the two failure modes calculated, OOP flexural bending tests were performed on horizontally spanning beams to evaluate the response of the constructed masonry under pure horizontal bending. This verification process along with further characterisation tests performed to understand the findings of this process are reported in Section 2.2.

2.2. Experimental verification of the design methodology

A total of four CS URM beams were tested in a four-point bending scheme, following the recommendations of EN 1052-2 [38]. Each of these beams were 1.76 m long, 0.56 m high and 0.102 m thick. In order to achieve a four-point bending loading scheme, the testing setup had two rollers supporting the beams symmetrically at a distance of 50 mm from their longitudinal edges. OOP flexural loading was applied via two symmetric rollers connected to an actuator applying the OOP load at a distance of 0.41 m from the support rollers. The adopted setup and loading scheme which is graphically illustrated in Fig. 1A resulted in the central part (0.88 m long in Fig. 1A) of the horizontal beam between the loading rollers to be a constant bending moment zone under pure horizontal bending as envisaged in a four-point bending test. Loading was applied in displacement control and each beam was densely instrumented with potentiometers not only to obtain experimental data allowing the construction of moment-normalized displacement curves but also in order to monitor that loading was applied with negligible eccentricities in a four-point bending scheme until failure.

Despite the design methodology adopted for the design of the unreinforced masonry (outlined in the previous section), all four horizontal beams tested under pure horizontal bending exhibited line-failure. Moment-normalized displacement curves for all four tested beams are also provided in Fig. 1B. Such a failure mode can also be observed to be associated with a sudden drop in strength as well as negligible resistance post realization of peak strength due to the absence of fracture along bed-joints and consequently the possibility of having torsional friction along these surfaces, contrary to stepped cracks. The moment provided in these moment-normalized displacement curves is the bending moment occurring in the constant bending moment region of the beam (as per simple statics applied to a beam under four-point bending) normalized by the height of the masonry beam, calculated as $M = (Fa/2)/h_w$ where F is the total force applied via both the rollers, a is the distance between the loading line and the supports i.e. 0.41 m in the adopted setup and h_w (= 0.56 m) is the height of the masonry beam. The normalized displacement Δ, was calculated by simply dividing the mid-span displacement by the distance from the support roller (= 0.85 m).

Such behaviour was most likely because of under prediction of the torsional response of masonry bed-joints under torsional shear by the equation developed by Willis ($\tau_{tor} = 0.9\sigma + 1.6f_{mt}$). A probabilistic treatment of the horizontal bending strength of URM is possible as per Vaculik [39] and the expected likelihood of WU-SJ (line) and SU-WJ (stepped) failures under pure horizontal bending can be calculated. However, even taking into account the variability observed for f_{mt} (Table 1) more than 80% likelihood of stepped failure is still calculated for the tested URM and pure WU-SJ behaviour rather than a combination of WU-SJ and SU-WJ behaviour was observed in all tested wallettes (Fig. 1B). An experimental procedure to measure the resistance of bed-joints under combined torsion and compression has already been presented by the same authors in [22]. As such results highlight the importance of further development of such a characterization test, this was performed again in this experimental campaign in order to experimentally verify the findings of the experiments subjecting URM beams to pure horizontal bending.

Tested specimens consisted of two CS bricks connected by a bed joint of reduced area (here 100x100 mm) in order to have the same overlap between bricks in tested URM beams as well as the full-scale specimen (Fig. 2A). Steel profiles rigidly connected to the test setup were used to prevent movement of the bottom brick. Vertical pre-compression on the mortar joint was applied through a thick steel plate resting on the upper brick. Dilation was not prevented by placing a soft deformable layer between this plate and the upper face of the top unit of the tested specimens. Gradually increasing horizontal loads (forming a force couple) were applied increasingly until failure of the specimens at a distance of 20 mm from the edge of the units to induce torsional

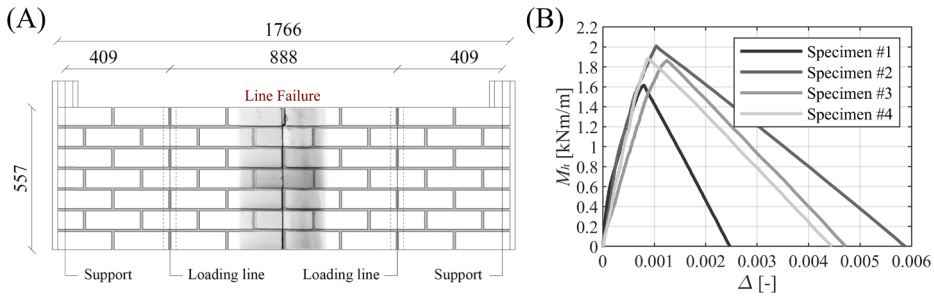

Fig. 1. Schematic of setup adopted for the tested beams and picture of line failure mode obtained in laboratory (A) and moment per unit height vs normalized displacement curves of beams tested under OOP flexural (B).

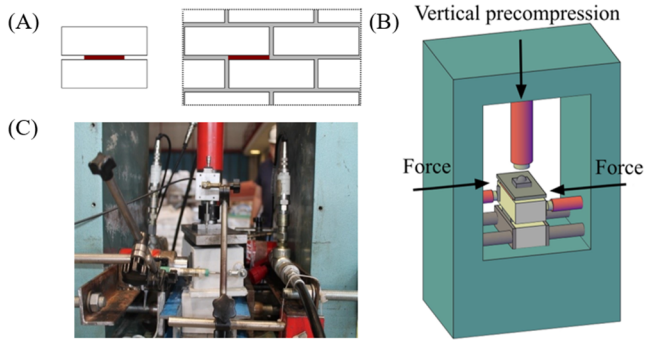

Fig. 2. Schematic showing why mortar joint of reduced area was used in tested masonry couplets (A) [22], idealized schematic of the adopted test setup (B) and setup for testing the torsional shear strength of bed joints in the laboratory (C).

shear in the mortar joint (Fig. 2B and Fig. 2C). Both horizontal displacements as well as uplift were monitored through the duration of the test. From the obtained experimental results, the strength of a masonry bed-joint under torsional shear (τ_{tor}) was evaluated using Eq. (5):

$$\tau_{tor} = \frac{T_{max}}{k_b \cdot 0.5 \cdot (l_u + t_j) \cdot t_u^2} \quad (5)$$

where T_{max} is the experimentally measured torque at failure of the masonry bed-joint. Eq. (5) is derived directly from 2: Eq. (2) provides the moment capacity of URM per unit crack length (M_h) while Eq. (5) evaluates the moment capacity of a single bed-joint of reduced area (T_{max}). Assumptions involved in Eq. (5) are: 1) the bed-joint of reduced area is a square elastic shaft and 2) maximum shear stress in the bed-joint occurs in the middle of both its edges [30]. Such assumptions can be deemed to be reasonable as 1) the torque-rotation behaviour of the masonry-couplets can be observed to be linear (Fig. 3A) and 2) this assumption allows a fair comparison of experimentally observed torsional-shear strength with that predicted with the equation for torsional shear strength developed by Willis [29] (who also adopted the same assumptions). Since the torsional shear tests were performed under three different levels of vertical stress (σ), a Coulomb-type friction law representation of the results is presented. The intercept and slope of a linear regression line passing through these points (τ_{tor}, σ) corresponds to values of cohesion ($f_{v0,tor}$) and friction coefficient (μ_{tor}) under torsional shear. The Coulomb-type friction law obtained from the experimental results is also compared with the torsional shear strength equation proposed by Willis in Fig. 3B.

Large intra-specimen variability in response can be observed in Fig. 3B. Such large variability was observed to be accentuated in the current study as well as in Graziotti *et al.* [22] when the predominant failure mechanism under torsional shear is associated with a failure surface passing through the thickness of the mortar joint as compared to the brick-mortar interface. A threshold in terms of τ_{tor} between SU-WJ (darker region) and WU- SJ (lighter region) has been provided in Fig. 3B. This threshold was calculated by adopting a value of f_{ut} = 2.61 MPa as per Table 1 in Eq. (3). The line separating the two regions thus represents the limiting value of τ_{tor} under different levels of σ separating the SU-WJ and WU-SJ configurations when the same CS units as this study and Graziotti *et al.* [22] are used. A value of $f_{v0,tor}$ equal to 1.37 MPa which is larger than the threshold τ_{tor} value of 0.65 MPa at 0 pre-compression load was measured experimentally. It can also be clearly observed in Fig. 3B that all tested specimens exhibited τ_{tor} values that were above the SU-WJ threshold as well as what is predicted using the relationship provided by Willis [29]. While this explains why the URM beams tested under horizontal bending exhibited line cracks instead of stepped cracks, even more importantly it places emphasis on the need for more investigations into the torsional shear strength of masonry bed-joints. A shift in masonry typology between WU-SJ and the SU-WJ typologies might have serious implications in OOP design and assessment of URM with the first typology offering very limited post-peak and residual capacity, something that was also very clearly observed in [22].

It is to be noted that currently in literature, very limited research [40,41] exists on the response of bed joints in masonry under torsional shear where the distribution of shear stress is non-uniform compared to the volume of work that exists on the behaviour of URM under the action of uniform shear stress at the brick mortar interface, and most of it is limited to dry-joint and not mortar bonded masonry. This is despite the fact that torsional shear resistance is one of the most important controlling parameters in virtual work based methods [42] that constitute existing state-of-the-art analytical formulation applied to URM loaded in the OOP direction. Though beyond the scope of this article, such an investigation should ideally involve both experimental studies at several scales (torsional couplets as well as wallettes in pure horizontal bending) with appropriate statistical considerations and accompanied by detailed numerical modelling calibrated with the obtained experimental data.

3. Full-scale specimens

This section of the article provides a brief overview of the full-scale specimens tested dynamically under OOP plane two-way bending excitation following the design methodology described until now. All specimens tested in this campaign were constructed with the same CS bricks measuring 212x102x71 mm used in [22]. Each wall consisted of 34 courses of masonry and masonry joints (both head and bed-joints) were 10 mm thick. This resulted in every wall being 2.75 m high. Other

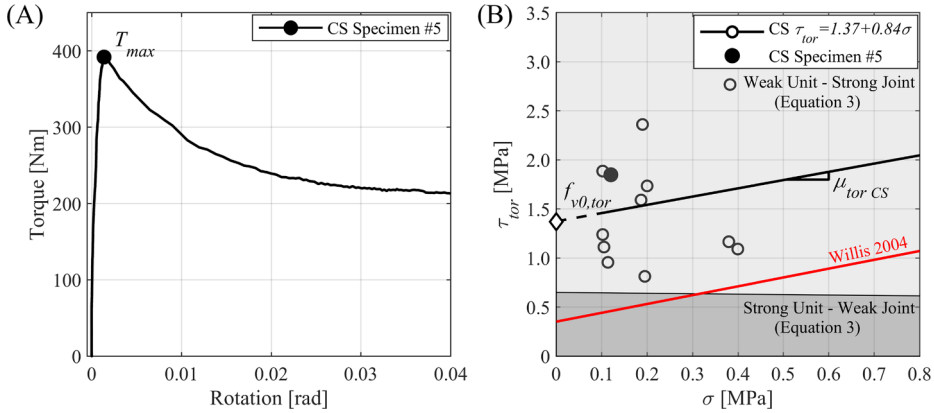

Fig. 3. Typical torque-rotation behaviour of a specimen (A) and comparison of Coulomb type friction law representation of results with τ_{tor} calculated as per Willis [29] (B).

than these similarities, all the four specimens differed among themselves in terms of geometry, support conditions or subjected excitation.

Each specimen consisted of an OOP wall and one or two return walls (depending on the envisaged boundary conditions). Two return walls were present for the first two specimens: CS-000-RFV, CS-000-RF2 (OOP wall weighing 2056 kg) which were tested with both vertical edges and the bottom horizontal edges completely restrained (fixed) and top horizontal edge free. These two U-shaped specimens differed only in terms of the fact that the adopted seismic excitation had a vertical component as well in case of the first specimen which is also reflected in the name adopted for it ("V" in CS-000-RFV). More details about the adopted input seismic excitation are provided in Section 4.2. The latter two specimens possessed one return wall each as they were envisaged to be tested with one each of both their vertical and horizontal edges unrestrained (free). This resulted in a L-shaped boundary condition configuration which is also reflected in the naming adopted for them: CS-000-L1 (OOP wall weighing 910 kg), CS-000-L2 (OOP wall weighing 1140 kg). These specimens differed only in terms of the length of their OOP panels and consequently in their aspect ratio.

It is to be noted that both of these specimens were constructed on the same foundation but separated by a gap of approximately 20 mm to avoid any interaction between them during dynamic tests. No vertical overburden was applied on the OOP panel of any of the tested specimens. The return walls of each of the specimens however were loaded with a vertical overburden of 0.05 MPa (Fig. 4). The grey regions on specimen CS-000-RF2 indicate where strips of plaster were applied externally to identify the earlier (if any) onset of damage on the plaster compared to the URM of the walls without affecting their structural response. Analytical formulation (along with experimental validation) accounting for the effect of plaster on the OOP two-way bending response of URM walls can be found in Derakshan *et al.* [43]. Similar to Graziotti *et al.* [22], idealized rather than realistic initial boundary conditions which can be found in a building stock were envisaged. This was in line with the motive to develop a repository of experimental data for developing and calibrating numerical models with.

4. Experimental setup and applied sequence of seismic excitation

4.1. Experimental setup

All specimens were tested on the 6-degrees-of-freedom shaking table of EUCENTRE, Pavia featuring a 4.8 × 4.8 m plan size and 30 t vertical payload capacity. Specimens were constructed on a reinforced concrete (RC) foundation. Connection between the bottom section of the wall and the RC foundation consisted of a mortar bed-joint. Steel bolts were used to anchor the RC foundation onto the shake table. Restraint along lateral vertical edges was achieved by the presence of perpendicular interlocking return walls. Interlocking was achieved by the presence of alternating rows of stretchers from the return walls and headers from the OOP panel. A gap of 30 mm was kept between the bottom of the blue steel beam (Fig. 5) and the top edge of the OOP panel in order to keep it free and unloaded as envisaged. Steel top beams were also placed on the return walls. These top beams were connected to a system of springs which were in turn connected (in series) to hollow cantilevers and bars.

The desired vertical pre-compression was achieved by pulling down this system of springs and consequently the top beams themselves (Fig. 5C). Calculations were performed to choose an appropriate stiffness of this system so as to ensure minimal increase of the applied overburden even at high levels of applied seismic excitation or damage states. The seismic input of the shaking table was transmitted to the upper portion of the loaded return walls. A rigid steel frame was placed on the shaking table to achieve this (Fig. 5A). The top beams of the return walls (which were pulled down to achieve the vertical pre-compression) were connected to this rigid frame by means of a steel beam (in blue in Fig. 5) anchored to the frame with steel braces. A system of steel profiles was used to restrain the OOP displacement of the return walls (i.e. in-plane direction of the tested OOP panels) and this system was connected to the rigid steel frame as well (Fig. 5B). Each specimen was instrumented with potentiometers and accelerometers. A 3D optical acquisition system was additionally used for recording displacements at an even larger number of locations. Instruments measuring displacement were placed based on expected deflected shapes of the walls. Instruments were also placed on various locations of the test setup described in the section in order to evaluate the efficiency of the adopted setup in inducing OOP two-way bending in the tested walls. For a more detailed description of the adopted test setup, the reader is referred to Graziotti *et al.* [22].

4.2. Input signals and testing sequence

Each specimen was subjected to a series of horizontal input motions in gradually increasing intensity until collapse. The employed input motions corresponded to three accelerograms recorded at the first floor level of a full-scale building tested at EUCENTRE [44]: FEQ1-DS0, FEQ2-DS3 and FEQ2-DS4. These floor accelerograms were obtained by adopting as dynamic input at the base of the structure two ground motions: EQ1 and EQ2, both considered representative of different hazard scenarios of the province of Groningen [45]. The second part of the name of the input motions refers to the damage state of the building when the floor accelerograms were recorded with DS0 referring to No Damage, DS3 to Moderate Damage and DS4 to Extensive Damage respectively. For example, FEQ1-DS0 refers to motions recorded at the first floor level when subjected to ground motion EQ1 scaled at 100%. The specimen CS-000-RFV was also subjected to vertical excitation simultaneously with the horizontal one. The applied vertical excitations were those recorded at the ground level, assuming consequently the building to be rigid in the vertical direction. No vertical excitation had been applied to any of the walls in Graziotti *et al.* [22]

Table 2 summarizes the information provided above about the seismic input used for testing the walls along with intensity measures characterising them, namely: peak table acceleration, velocity and displacement (*PTA*, *PTV* and *PTD*) Arias intensity (I_A), modified Housner intensity (*mHI*) and the spectral acceleration associated with the records at a period of 0.1 s i.e. around the fundamental period of the tested specimens (Table 4). In Table 2, peak ground acceleration (*PGA*) is a characteristic of the ground motion from which the applied seismic input was obtained from while *PTA* corresponds to the peak

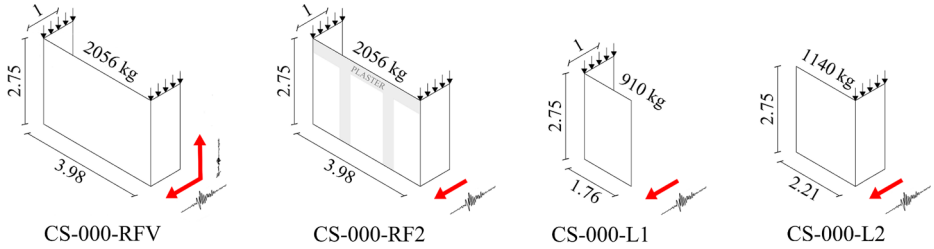

Fig. 4. Specimen geometries, masses and directions of applied input (grey regions on specimen CS-000-RF2 indicate where strips of plaster were applied).

Fig. 5. General view of the adopted testing setup (A), return wall restraint system (B) adopted system for the applying overburden pressure to the return walls (C), CS-000-RF2 (strips of plaster were applied to this specimen) (D) and CS-000-L1&L2 (E).

acceleration recorded when the same ground motions were applied scaled at the desired level.

Acceleration time histories (scaled at 100%) along with both displacement and acceleration (5% damped) spectra associated with the applied horizontal and vertical seismic input are provided in Fig. 6. In addition to the employed seismic input mentioned above, very low intensity excitations having a broad frequency range (specified as RN in Table 3) were performed in between tests to evaluate the dynamic properties of walls and detect changes in them if any (indicating the occurrence of damage).The incremental dynamic testing sequence adopted for each specimen along with respective scaling factors (S.F.), measured peak table accelerations (*PTA*) and peak wall displacements (*TD*) are summarized in Table 3. For all specimens CS-000-RFV, CS-000-RF2 *TD* is recorded at the mid-point of the unrestrained top edge for and for CS-000-L1, CS-000-L2 on top of the unrestrained vertical edge. The test marked in bold letters for CS-000-RFV and CS-000-L2 is the run of the test sequence after which initial occurrence of damage was observed. No damage was observed for CS-000-RF2 prior to collapse. The values of S.F. provided were calculated as the ratio of the spectral acceleration at the fundamental period of the wall (obtained from random excitation tests and provided in Table 4) in a spectrum calculated from an accelerometer recording at the RC foundation to the spectral acceleration at the same period in the spectrum of the unscaled seismic input.

5. Testing results

Results of the full-scale dynamic experiments are presented and discussed in terms of: fundamental mode of vibration of the walls and its evolution; three dimensional deformed shapes constructed for tests at the instants in which the OOP panel had peak displacement; pictures of progression of damage in the walls along the incremental dynamic testing sequence; failure mechanisms and how they compare to expected mechanisms as per their envisaged boundary conditions in literature; force-displacement hysteretic behaviour. The same sequence of damage states used for presenting the results in Graziotti *et al.* [22] are used again (shown qualitatively in Fig. 7): DS1 corresponding to no visible structural damage, DS2 to slight structural damage, DS3 to moderate damage with full development of the collapse mechanism, DS4 to heavy damage with negligible residual capacity and ultimately DS5 corresponding to very heavy damage associated with global or partial collapse of the panel. Other than CS-000-L2 which remained in DS1 throughout the testing sequence, all other specimens were tested up to DS5.

Table 2
Employed seismic input characteristics (scaling factor = 1).

Input	GM input		Horizontal						Vertical					
		GM *PGA* [g]	*PTA* [g]	*PTD* [mm]	*PTV* [mm/s]	I_A [mm/s]	*mHI* [mm]	S_a (0.1 s) [g]	*PTA* [g]	*PTD* [mm]	*PTV* [mm/s]	I_A [mm/s]	*mHI* [mm]	S_a (0.1 s) [g]
FEQ1-DS0	EQ1-100%	0.10	0.13	7	63	58	150	0.20	0.07	3	16	15	50	0.22
FEQ2-DS3	EQ2-125%	0.19	0.23	24	171	296	462	0.33	0.10	24	54	143	183	0.27
FEQ2-DS4	EQ2-200%	0.31	0.33	46	309	784	969	0.37	0.15	39	86	366	292	0.43

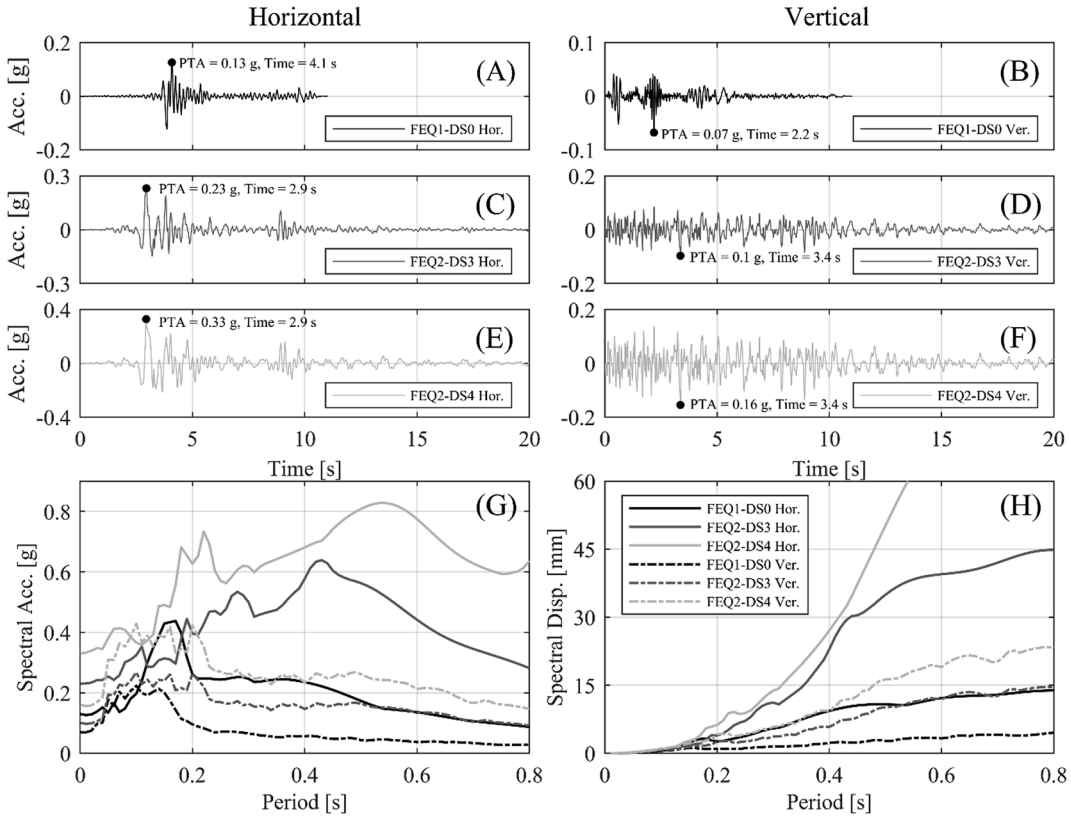

Fig. 6. Acceleration time histories of the employed horizontal vertical input motions FEQ1-DS0, FEQ2-DS3, FEQ2-DS4 (A-B, C-D, E-F), 5% damped acceleration (G) and displacement (H) response spectra.

Table 3
Testing sequences adopted for incremental dynamic testing of the specimens.

	CS-000-RFV					CS-000-RF2				CS-000-L1&L2					
T#	Test Input	S.F.	*PTA H* [g]	*PTA V* [g]	*TD* [mm]	Test Input	S.F.	*PTA* [g]	*TD* [mm]	Test Input	*PTA* [g]	S.F. L1	*TD* L1 [mm]	S.F. L2	*TD* L2 [mm]
1	RN X	–	−0.07	+0.04	–	RN	–	+0.08	–	RN	+0.04	–	–	–	–
2	RN Z	–	+0.04	−0.12	–	FEQ1-DS0	65%	−0.07	+0.3	FEQ1-DS0	−0.07	70%	+0.34	50%	−0.6
3	RN X-Z	–	+0.02	−0.02	–	FEQ1-DS0	130%	−0.11	+0.5	FEQ1-DS0	−0.10	110%	+0.42	70%	+0.8
4	FEQ1-DS0	55%	−0.06	+0.05	+0.4	FEQ1-DS0	110%	−0.12	+0.5	FEQ1-DS0	+0.11	100%	+0.48	90%	+1.0
5	FEQ1-DS0	80%	−0.10	+0.07	+0.5	FEQ1-DS0	160%	+0.15	+0.5	FEQ1-DS0	−0.14	110%	+0.44	100%	−1.1
6	FEQ1-DS0	110%	−0.12	+0.10	+0.6	FEQ1-DS0	150%	+0.17	+0.5	FEQ1-DS0	+0.16	140%	+0.53	130%	−1.3
7	FEQ1-DS0	120%	+0.15	−0.11	+0.6	FEQ2-DS3	60%	+0.14	+0.7	FEQ2-DS3	+0.14	60%	−0.80	70%	−1.4
8	FEQ1-DS0	140%	+0.17	+0.10	−0.7	FEQ2-DS3	90%	+0.22	+1.4	FEQ2-DS3	+0.22	100%	+1.54	100%	−2.8
9	FEQ2-DS3	70%	+0.15	+0.11	−0.8	FEQ2-DS3	130%	+0.26	+1.6	RN	+0.06	–	–	–	–
10	FEQ2-DS3	120%	+0.20	+0.11	−1.3	FEQ2-DS4	80%	+0.26	+1.4	FEQ2-DS3	+0.25	110%	−1.72	110%	−3.7
11	FEQ2-DS3	115%	+0.26	+0.11	−1.5	FEQ2-DS4	90%	+0.36	−1.4	FEQ2-DS4	+0.29	80%	+1.64	110%	+3.2
12	FEQ2-DS4	85%	+0.28	+0.11	+1.5	FEQ2-DS4	140%	+0.43	−2.2	FEQ2-DS4	+0.36	100%	−1.61	120%	−2.9
13	FEQ2-DS4	105%	+0.34	+0.15	+1.7	FEQ2-DS4	140%	+0.43	−2.5	FEQ2-DS4	+0.42	140%	−2.37	120%	−2.8
14	FEQ2-DS4	125%	+0.40	+0.18	−2.2	RN	–	−0.07	–	FEQ2-DS4	+0.47	150%	−2.61	120%	−3.4
15	FEQ2-DS4	145%	+0.46	−0.24	−2.6	FEQ2-DS4	175%	+0.52	−3.0	FEQ2-DS4	+0.49	170%	−3.17	160%	−5.0
16	FEQ2-DS4	170%	+0.54	+0.19	−2.7	FEQ2-DS4	210%	+0.78	−6.2	RN	+0.07	–	–	–	–
17	FEQ2-DS4	220%	+0.78	−0.27	−3.8	RN	–	−0.07	–	**FEQ2-DS4**	**+0.75**	250%	−4.90	**300%**	**−10.5**
18	FEQ2-DS4	235%	+0.89	−0.65	−4.3	FEQ2-DS4	250%	+0.90	−8.2	RN	+0.08	–	–	–	–
19	RN X	–	+0.07	−0.05	–	**FEQ2-DS4**	**360%**	**+1.03**	**Fail.**	**FEQ2-DS4**	**+0.91**	270%	−6.91	**320%**	**Fail.**
20	**FEQ2-DS4**	**335%**	**−1.07**	**−0.51**	**−6.6**										
21	RN X	–	+0.05	+0.04	–										
22	FEQ2-DS4	120%	+0.31	+0.21	−2.1										
23	FEQ2-DS4	150%	+0.51	+0.31	−4.0										
24	FEQ2-DS4	250%	+0.65	−0.50	−6.4										
25	RN X	–	+0.07	−0.05	–										
26	FEQ2-DS4	255%	+0.76	−0.52	−10.7										
27	RN X	–	−0.07	+0.05	–										
28	**FEQ2-DS4**	**305%**	**+0.92**	**−0.55**	**Fail.**										

Table 4
Dynamic identification of the first natural mode of vibration of the specimens.

CS-000-RFV			CS-000-L1			CS-000-L2			CS-000-RF2		
T# DSi	Freq. [Hz]	*T* [s]	T# DSi	Freq. [Hz]	*T* [s]	T# DSi	Freq. [Hz]	*T* [s]	T# DSi	Freq. [Hz]	*T* [s]
1 DS1	12.4	0.080	1 DS1	12.5	0.080	1 DS1	10.1	0.099	1 DS1	12.8	0.078
19 DS1	11.3	0.088	9 DS1	12.3	0.081	9 DS1	9.8	0.103	14 DS1	12.1	0.083
21 DS2	9.9	0.101	16 DS1	11.5	0.087	16 DS1	9.4	0.107	17 DS1	11.3	0.089
25 DS2	8.2	0.122	18 DS1	11.5	0.087	18 DS2	9.0	0.111			
27 DS3	7.6	0.132									

5.1. Dynamic identification

Dynamic properties, in particular the first natural mode of vibration of each tested specimen was continuously monitored throughout the testing sequence. A major motivation behind doing this was the fact that a change in the dynamic properties is indicative of damage, which sometimes could not be documented by visual observation. In order to achieve this, the entire testing sequence was interspersed with low amplitude vibration runs (identified as RN in the testing sequence in Table 3) encompassing a broad range of frequencies.

5.2. Damage patterns and failure mechanisms

This section summarises visual observations of damage made for all tested full-scale specimens throughout their incremental dynamic testing sequence. All observed damage is classified as per one of the damage states shown in Fig. 7. It is to be noted that the positive and negative directions referred to in this section (especially while providing the 3D deformed shapes) refer to the directions normal to the OOP panel towards and away from the return walls respectively. Videos documenting the failure of each specimen can be found online at [46].

5.2.1. Calcium Silicate walls free on top (CS-000-RFV and CS-000-RF2)

Specimen CS-000-RFV was subjected to simultaneous horizontal and vertical excitation. It remained undamaged until Test #20 (*PTA H* = 1.07 g, *PTA V* = 0.51 g, peak *TD* = 6.6 mm) when it attained DS2. First cracking consisted of a vertical crack at the intersection of the OOP panel and right return wall developing from a height of approximately 1 m from the bottom up to the top edge of the wall. Additionally, cracks could also be seen in the upper left corner of the OOP panel as well as the left return wall (Fig. 8A). Deformed shapes in both positive and negative directions were very similar. High displacements were observed along the entire free top edge with the lower part of the OOP panel remaining relatively immobilized (Fig. 8E).

More damage was observed in Test #24 (*PTA H* = 0.65 g, *PTA V* = 0.50 g, peak *TD* = 6.4 mm) with an additional vertical line crack appearing in the centre of the OOP panel. This crack also extended to the top edge of the wall from the same height as the crack at the intersecting edge of the OOP panel with the right return wall. Despite the increase in observed damage as well as change in dynamic properties (Table 4) the specimen can be still considered to be in DS2 as DS3 was reached only in Test #26 (*PTA H* = 0.76 g, *PTA V* = 0.52 g, peak *TD* = 10.7 mm). This test saw the development of a horizontal crack from the base of the central line crack towards the left return wall. A diagonal crack also extended from the same crack towards the left return wall. Deformed shapes provided from Test #26 which can be considered representative of the occurring failure mechanism (Fig. 8F) show a shift of maximum displacements along the entire top edge to being localized along the central vertical section of the OOP panel corresponding to the formation of the central line crack. Relatively less displacement can also be observed for the part of the panel below the horizontal crack. The specimen collapsed (DS5) during Test #28 (*PTA H* = 0.92 g, *PTA V* = 0.55 g). Collapse of the specimen occurred by development of another line crack at the connection with the right return wall and the consequent overturning of the OOP panel about a horizontal crack passing through the base of all three vertical line cracks. Additional horizontal and diagonal cracking was observed at the portion of the wall below the panels which overturned. The cracks leading to the activation of the failure mechanism have been reproduced in blue in Fig. 8C from a careful examination of the video of the ultimate test. Fig. 8G-H illustrate instead snapshots of the video documenting the exhibited collapse mechanism.

Considering the very fast progression of damage states observed specimens tested in the same boundary condition i.e. CS-000-RFV as well as CS-000-RF in [22], strips of plaster were put on specimen CS-000-RF2 to discover the earlier onset of damage states on the plaster with respect to the URM. However, CS-000-RF2 remained in DS1 until the ultimate test and interestingly the plaster also did not exhibit any damage till then. This non-occurrence of damage is also confirmed by its dynamic properties remaining constant throughout the testing sequence and reported in Table 4. CS-000-RF2 reached DS5 progressing through all other damage states in Test#19. The crack pattern that triggered the failure mechanism is illustrated in Fig. 9A. The failure mechanism involved almost the entire OOP panel from a height of 0.6 m (see Fig. 9C). However, overturning of only the upper portion of the OOP panel took place (around a crack at a height of 1.5 m, see Fig. 9E) due to the presence of wire potentiometers which had not been removed. The instrumentation held back the lower portion of the panel (region in grey in Fig. 9A and E) involved in the failure mechanism as it can be clearly seen in Fig. 9D–E.

A total of three walls with the same geometries and boundary conditions, namely: CS-000-RF [22], CS-000-RFV and CS-000-RF2 have been tested in this experimental campaign, allowing the possibility of having conclusive information about the OOP behaviour of walls in this

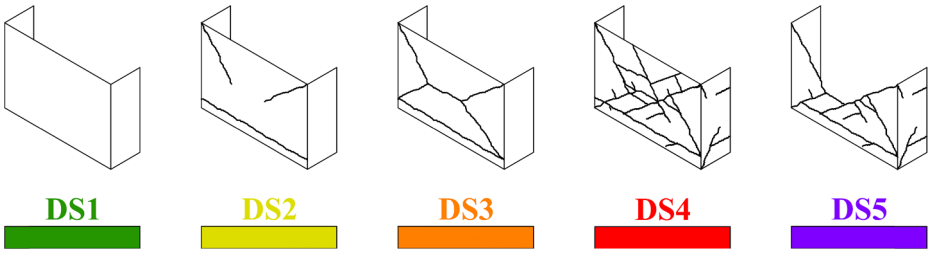

Fig. 7. Qualitative representation of damage states used to describe the progression of damage in the specimens [22].

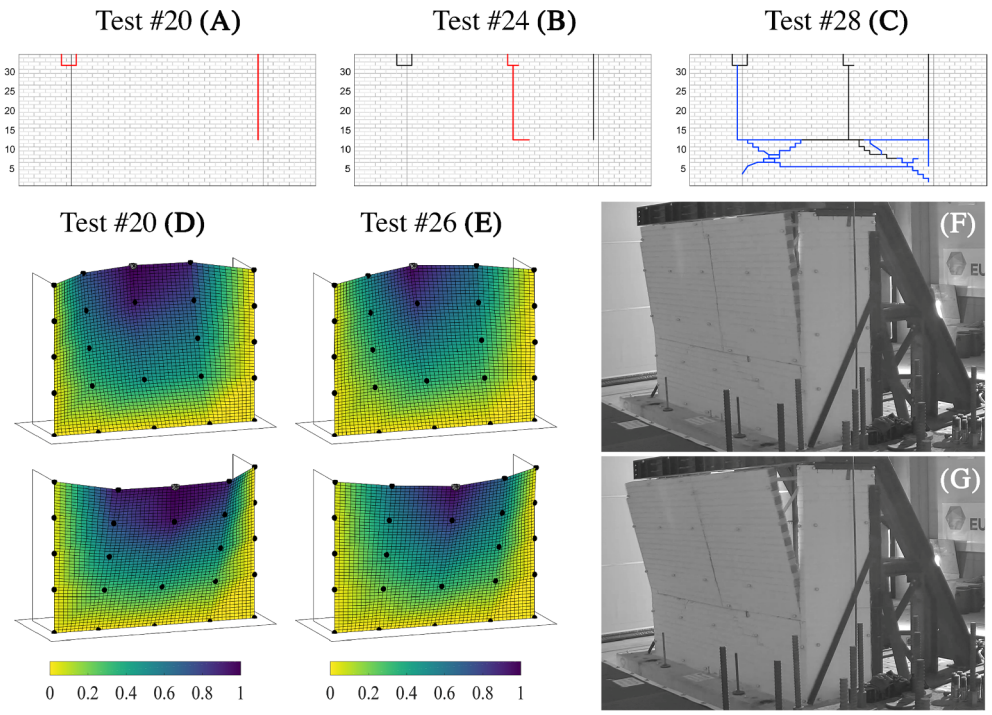

Fig. 8. CS-000-RFV: evolution of damage (A-C); deformed shapes in positive and negative directions: (Test #20, *PTA H* = −1.07 g, *PTA V* = 0.51 g, peak *TD* = +6.2 mm/−6.6 mm) (D), (Test #26, *PTA H* = 0.76 g, *PTA V* = −0.52 g, peak *TD* = +6.2 mm/−10.7 mm) (E); development of specimen collapse mechanism (F-G).

configuration. It was observed that development of the failure mechanism took place in an identical manner for all three specimens. Vertical cracks always appeared first at the connection of the OOP panel with the return walls. This was accompanied simultaneously or followed by the development of a vertical crack near the centre of the panel. Ultimately, failure in all three specimens took place by overturning of the part of the OOP panel bounded by these vertical cracks. The slight difference in rate of progression in damage observed in the three specimens is attributed to the mode of testing adopted i.e. incremental dynamic testing and progression of scaling factors employed.

5.2.2. Calcium Silicate walls free on top and along one vertical edge (CS-000-L1 and CS-000-L2)

CS-000-L1 which corresponded to a shorter OOP panel, remained in DS1 throughout the entire testing sequence. CS-000-L2 reached DS2 in Test #17 (*PTA H* = 0.75 g, peak *TD* = 10.5 mm) but initiation of cracking was restricted to a vertical line crack in the vicinity of the connection of the OOP panel with its return wall (Fig. 10A). CS-000-L2 ultimately reached DS5 in Test 19. Collapse of the specimen occurred via extension of the existing vertical line crack and consequent overturning of the OOP panel as well as a portion of the return wall about a horizontal crack approximately 1.1 m from the base of the wall (Fig. 10B). This is illustrated in Fig. 10E. Deformed shapes of both specimens exhibited a concentration of high displacements above a diagonal connecting the extremities of the free edges to the extremities of the fixed edge (Fig. 10C and D).

5.3. Hysteretic behaviour and incremental dynamic testing sequence

The hysteretic behaviour exhibited by the tested specimens is

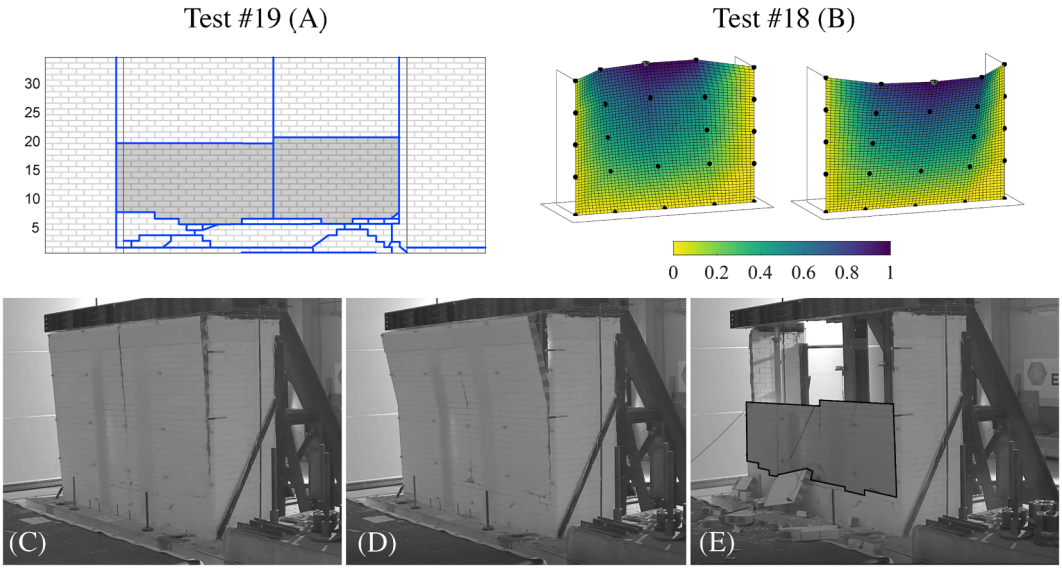

Fig. 9. CS-000-RF2: crack pattern at Test #19 (A); deformed shapes in positive and negative directions: (Test #18, *PTA* = 0.90 g, peak *TD* = +2.8 mm/−8.2 mm) (B); development of specimen collapse mechanism (C-E): region in grey indicates portion of OOP panel prevented from overturning by the used instrumentation.

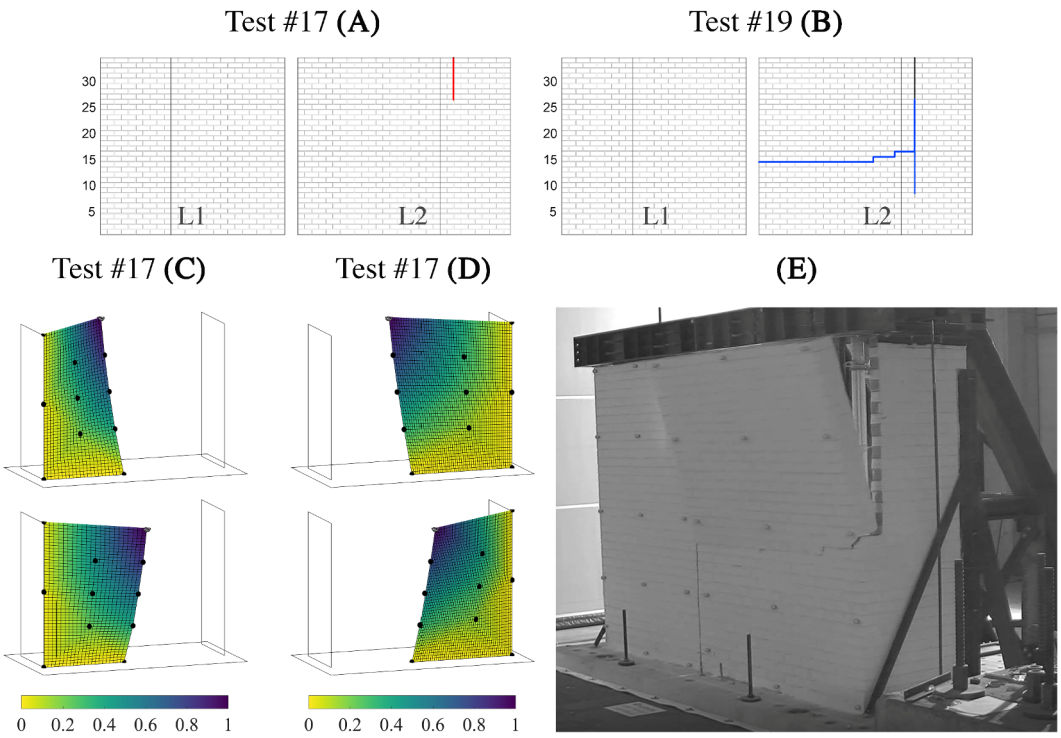

Fig. 10. CS-000-L2: evolution of damage (A-B); deformed shapes in positive and negative directions: L1 portion (Test #17, *PTA* = 0.75 g, peak *TD* = +2.1 mm/−4.9 mm) (C), L2 portion (Test #17, *PTA* = 0.75 g, peak *TD* = +4.9 mm/−10.5 mm) (D); development of specimen collapse mechanism (E).

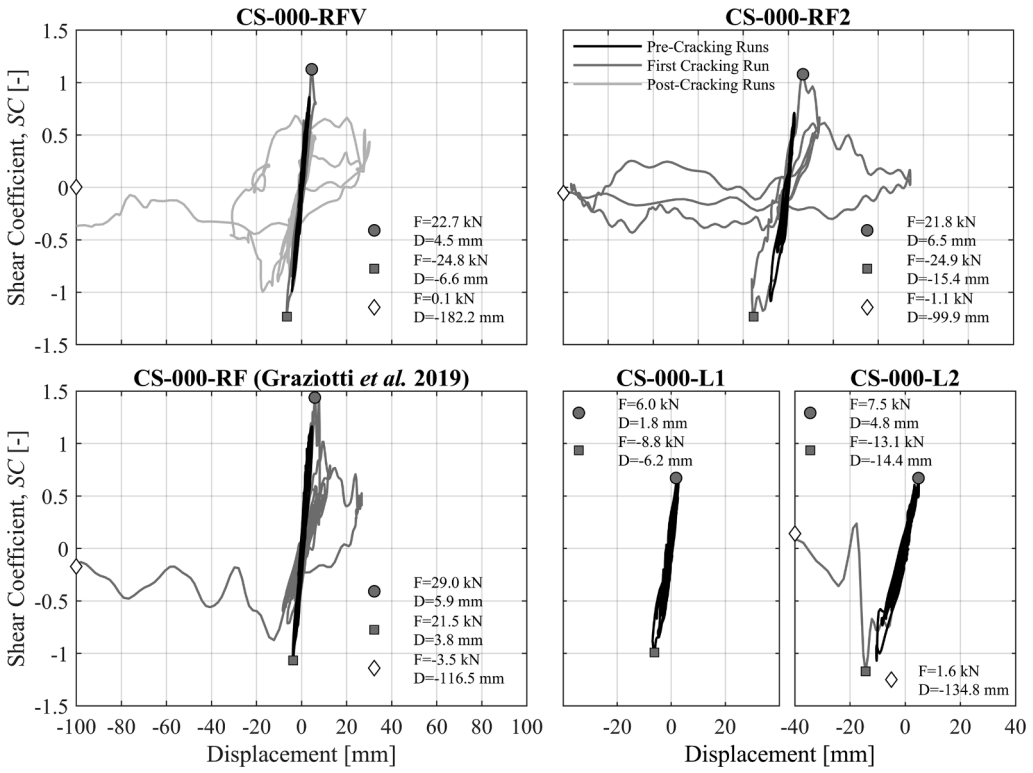

Fig. 11. Hysteretic response of every specimen: circular and rectangular markers identify attainment of peak forces in positive and negative directions respectively; diamond marker indicates force and displacement at the location where recording has been terminated for specimens tested up to DS5.

illustrated in Fig. 11. Comparison between specimens having different masses has been facilitated by providing these results in the form of shear coefficient *(SC)* rather than the inertial forces directly. The *SC* provided in Fig. 11 was calculated by dividing the inertial force associated with each wall by the mass of its OOP panel and *g* (acceleration due to gravity). Inertial forces associated with the walls were calculated by assuming the mass of the OOP panel to be lumped at the recording accelerometers. The tributary mass associated with each accelerometer was changed within the testing sequence (if required) to take into account the damage state of the specimen. For all specimens,

displacements provided here (named *TD*-Top displacement) are recorded at the mid-point of the unrestrained top edge for CS-000-RFV, CS-000-RF2 and on top of the unrestrained vertical edge for CS-000-L1, CS-000-L2.

On the basis of observed progression of damage states, the response of each specimen has been separated into three phases each of which is plotted with different colors: pre-cracking, first cracking and post cracking tests. The pre-cracking phase corresponds to tests in which the specimens remained in DS1. Very similarly to the four specimens constructed in CS masonry tested in Graziotti *et al.* [22], all specimens tested in this phase also exhibited very brittle behaviour. This can be attributed to the fact that CS masonry tested in both phases corresponded to a "WU-SJ" configuration. In fact, the progression from DS3 to DS5 for specimens CS-000L2 and from DS1 to DS5 for CS-000-RF2 occurred in a single run of the testing sequence. Even for CS-000-RFV, a transition from DS3 to DS5 occurred in consecutive runs (separated by RN test performed to evaluate the change in dynamic properties). This is indicative of the very quick stiffness and strength degradation that took place for all the specimens and can also be noticed clearly in their hysteretic behaviour as shown in Fig. 11.

CS-000-L1 remained in DS1 throughout the entire testing sequence and the same is reflected in its hysteretic behaviour. Peak inertial force for CS-000-L2 was sustained up to displacements of around 14 mm compared to CS-000-RFV (around 6 mm) but this is expected because of its boundary condition i.e. having an additional vertical edge free. Specimens CS-000-RFV and CS-000-RF2 attained a very similar peak inertial force of 25 kN. In comparison, specimen CS-000-RF (having same geometry and boundary conditions) tested in [22] attained a slightly higher peak inertial force of 29 kN; this difference is likely due to the inter-wall (different mechanical properties with respect to the current campaign) and intra-wall intrinsic variability associated with URM that caused a larger height of the OOP panel to be involved in its failure mechanism. Specimens CS-000-RF and CS-000-RFV attained peak inertial force at very similar displacements of approximately 6 mm. For CS-000-RF2, this value was much higher at approximately 15 mm. However, this is because of the even faster progression of damage states in CS-000-RF2 as compared to the other two specimens: CS-000-RF2 exhibited peak force response and went from DS1 to DS5 in a single run of the testing sequence. No effect of the applied vertical excitation could be observed on the response of CS-000-RFV when compared to CS-000-RF2 and CS-000-RF. However, this is mainly attributed to the fact that that the peak strength of all these walls was controlled by the flexural tensile strength of used masonry units which is hardly affected by the acting axial load and also due to the difference in frequency content of applied vertical and horizontal seismic excitation (Fig. 6G and H).

Fig. 12 compares peak table accelerations (*PTA*) at which first cracking and collapse occurred for CS-000-RR tested in [22] with all four edges restrained with those of CS-000-RF [22], CS-000-RFV,CS-000-RF2 which were tested with three edges restrained. Comparison is also done with the OOP two-way bending collapse of a wall in a full scale building incrementally dynamically tested as a part of the same project by Tomassetti *et al.* [47]. *PTA* values are somewhat lower for the collapse observed in the building to walls tested alone but this can be attributed to the higher length of the OOP panel. This wall ([47]) along with CS-000-RF2 were also the only walls which underwent first cracking and collapse in the same run of the testing sequence i.e. *PTA* at collapse is equal to *PTA* at first cracking.

6. Interpretation of the experimental results

6.1. Predictions of peak strength

Predictions of peak strength of the walls tested in the current study were again done using all different approaches adopted in Graziotti *et al.* [22]. All of these methods use the codified form of the virtual work method provided in the Australian standard for masonry structures (AS 3700) [32] which calculates the peak strength of URM walls in OOP two-way bending as per Eq. (6):

$$q = \frac{2a_f}{{L_d}^2}(k_1 M_h + k_2 M_d) \tag{6}$$

In Eq. (6): q is the peak strength of the wall calculated as a uniformly applied wall face pressure; M_h and M_d denote moment capacities associated with horizontal and diagonal bending per unit crack length; L_d is the effective length of the wall which depends on its boundary conditions and the presence or absence of an opening; k_1, k_2 and a_f are coefficients dependent on wall geometry and boundary conditions. Formulas for calculating L_d, k_1, k_2 and a_f are provided in a tabular form based on wall geometry, support conditions and presence/absence of openings in AS 3700 [32]. The results of analytically calculated peak strengths are compared to experimental results in Fig. 13 again in terms of shear coefficient *(SC)*.

The different approaches reported in this section only differ in terms of the moment capacity equations used for horizontal (M_h) and diagonal bending (M_d). All methods also ignore the contribution of vertical bending to the two-way bending strength of URM walls. The different moment capacity equations used were the ones provided in AS 3700 (SC_{AS}) [32], equations proposed by Griffith and Vaculik [28] (SC_{GV}) and also the same equations used to calculate SC_{GV} but replacing the torsional shear strength of masonry with ultimate torsional shear stress relationships derived from experimental torsional shear testing ($SC_{GV\tau}$)

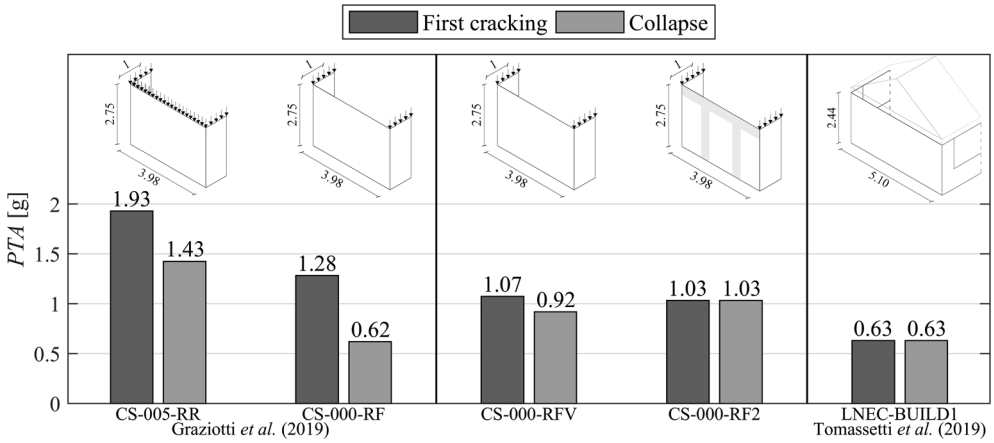

Fig. 12. Peak table acceleration (*PTA*) at which first cracking and collapse occurred for walls in different boundary conditions in standalone situations and in a building [47].

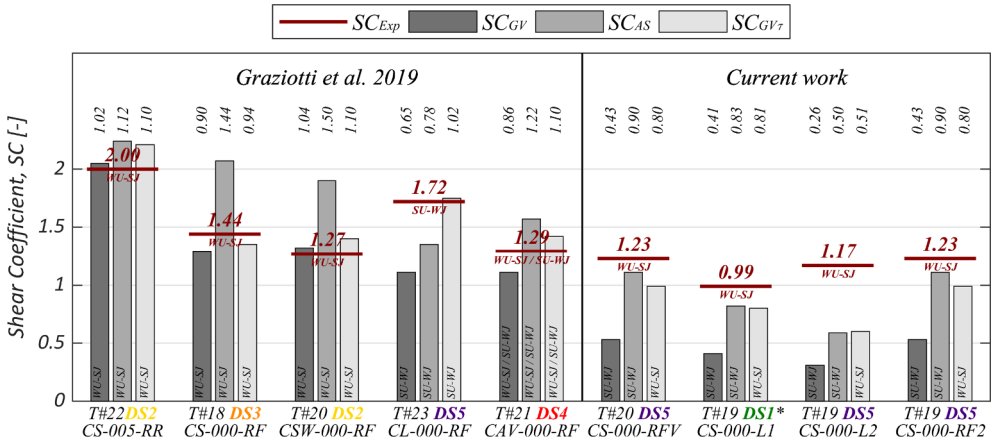

Fig. 13. Predictions of peak force resistance for specimens tested in current work and Graziotti *et al.* [22].
*Specimen CS-000-L1 did not sustain any damage throughout its testing sequence and consequently the SC_{Exp} reported here could be lower than its actual peak strength.

provided in Section 2.2. Also, as per the recommendations of Griffith and Vaculik [28] and similar to [22], all calculations take into account only 50% of the horizontal bending moment capacity arising at connections with the return wall towards the peak strength of the wall. Unlike what was observed in Graziotti *et al.* [22], the values of SC_{GV} compare very unfavourably low to SC_{Exp}. But this is expected as the moment capacity equations developed by Griffith and Vaculik use the torsional shear strength relationship developed by Willis [29] which predicts the tested URM as SU-WJ instead of WU-SJ under pure horizontal bending (explained in Section 2.2). It is important to note here that while AS 3700 (SC_{AS}) strength predictions compare well to experimental results in the current study, the used empirical moment capacity equations again predict the tested URM to be SU-WJ rather than WU-SJ. A correct identification of the WU-SJ failure mode and a consequent improvement in these predictions for all the walls tested in this study as well as in [22] is observed when these moment capacity equations use the ultimate torsional stress relationship obtained experimentally (Section 2.2) i.e. $SC_{GV\tau}$ (Fig. 13).

6.2. Predictions of initial stiffness and wall displacement at peak strength

In Section 6.1 and Graziotti *et al.* [22], focus was placed primarily on estimating the OOP peak inertial force resisted by walls under two-way bending implementing analytical formulation based on the virtual work method. Since the implemented formulation was very satisfactorily able to estimate the force resistance offered by the tested walls and considering the limited post peak resistance observed for the tested walls, what has been missing from this framework is a simplified method for calculating the displacement at which such peak inertial force resistance is achieved or rather the initial elastic stiffness of walls under OOP two way bending. This section of the article overcomes this shortcoming by providing analytical formulation based on the theory of plates [48] to estimate the initial stiffness of the walls tested in [22] as well as this experimental campaign. Similar to the methodology adopted to calculate the peak force resistance of the walls, the external dynamic loads are assumed to be acting in the form of a uniformly applied pressure on the wall. Adopting this assumption also allows combination of the procedure proposed to calculate the peak inertial force of a wall panel in [22] with the methodology proposed in this section into an unified framework for calculating the stiffness and peak force resistance associated with URM panels under OOP two-way bending excitation. Formulation to calculate the maximum displacement (TD) of rectangular plates at various locations on their edges under a given uniformly distributed load and different boundary conditions are typically provided in [48] and [49] in the form of Eq. (7):

$$TD = \frac{\alpha \cdot q \cdot x^4}{D} \text{ where } D = \frac{E \cdot t^3}{12(1-\nu^2)} \tag{7}$$

In Eq. (7), α is a numerical factor that depends on the boundary condition of the plate (i.e. here the OOP panel) as well as its aspect ratio, q is the uniform lateral load assumed to be acting on the wall (same quantity as in Eq. (6)) and D is the flexural rigidity of the plate/OOP panel. To calculate D: E refers to the modulus of elasticity of the material in tension and compression, t to the thickness of the plate and ν to the Poisson's ratio of masonry. It is important to note that in Eq. (7), for walls restrained on all four edges (e.g. CS-005-RR [22]) or just two adjacent edges (e.g. CS-000-L2), x refers to the shorter among the wall dimensions (l or h) while for walls restrained on only three edges (e.g. CS-000-RF2) it refers to the dimension of the unrestrained edge (l). Analytical solutions and consequently values of α (Eq. (7)) corresponding to walls supported on all four edges (as in the case of CS-000-RR [22]) as well as walls supported on all three edges (as in the case of CS-000-RFV and CS-000-RF2) are provided in [48]. However, for the problem of bending of walls with two adjacent edges fixed or simply supported and the other two adjacent edges free reference was made to a newer study on the bending of rectangular plates based on a sympletic approach [49]. These solutions are very interesting as they allow calculation of limiting values of the initial stiffness of walls in almost all practically encountered boundary conditions.

Eq. (7) was consecutively used to predict the displacement of all walls tested in [22] as well as this campaign. The value of E used in these predictions were experimentally obtained from compression tests on masonry wallettes (Table 1). These predictions were done in both the elastic phase of the wall i.e. when all specimens were in DS1 as well as at the instant of attainment of peak strength. For both scenarios i.e. elastic and the attainment of peak-strength these calculations were done assuming all restrained edges to be completely fixed (FF) as well as simply supported (SS). An edge-fixity factor β was evaluated for every specimen as per Eq. (8):

$$\beta = \frac{TD_{exp} - TD_{FF}}{TD_{FF} - TD_{SS}} = \frac{\alpha_{exp} - \alpha_{FF}}{\alpha_{FF} - \alpha_{SS}} \tag{8}$$

In Eq. (8), TD_{exp} is the experimentally recorded displacement while TD_{FF} and TD_{SS} are the FF and SS predictions respectively. α_{exp} is computed by inverting Eq. (7) to obtain TD_{exp} while α_{FF} and α_{SS} can be found in [48,49]. Under the assumption that the experimental displacements always lie between the FF and SS scenarios, β can vary between 0 and 1, with a value of 0 indicating that TD_{exp} is the same as TD_{FF} i.e. the boundary conditions at the restrained edges correspond to a completely fixed situation while a value of 1 indicates the contrary i.e. boundary conditions at the restrained edges correspond to a simply

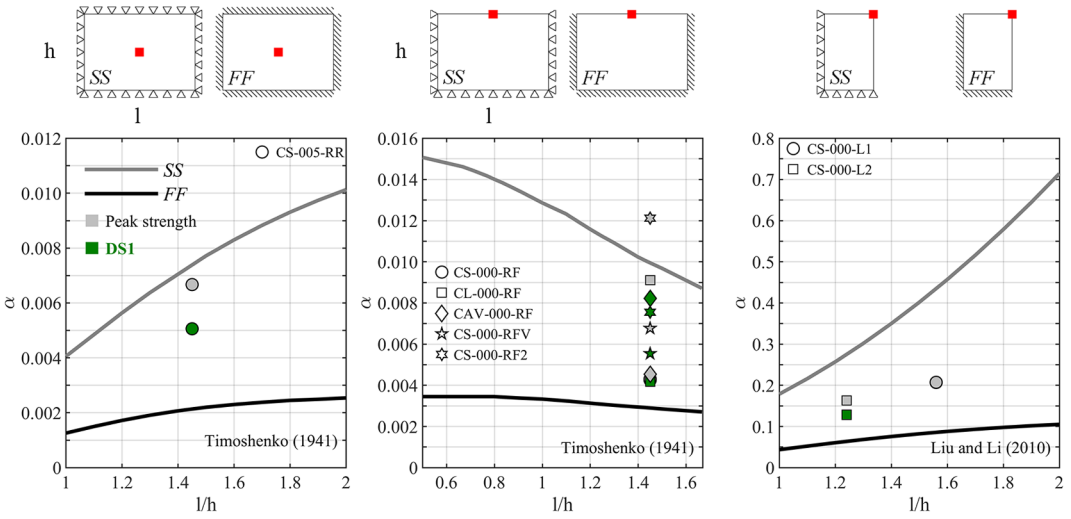

Fig. 14. Charts for calculating α (in Eq. (7)) for varying aspect ratio (height/span) of walls under limiting boundary conditions (simply supported, *SS* and fixed, *FF*) at location specified by red square along with α_{exp} values required to obtain the value of TD_{exp} recorded for all tested specimens in both DS1 and at the attainment of peak strength (For interpretation of the references to colour in this figure legend, the reader is referred to the web version of this article.)

supported situation.

It was observed that TD_{exp} of all specimens tested in the current study and [22] lie well within the range specified by TD_{FF} and TD_{SS} in the elastic phase / DS1. At the instant of attainment of the peak strength, displacement of all specimens other than CS-000-RF2 again lie well within the limits prescribed by TD_{FF} and TD_{SS}. This different observation in the case of CS-000-RF2 is best attributed to the fact that CS-000-RF2 was the only specimen that jumped from DS1 to DS5 in a single run of the testing sequence. It also exhibited a much higher (almost double) displacement compared to the two other specimens tested in the same configuration across the experimental campaign. All these results are provided in terms of α_{exp} in Fig. 14.

The edge-fixity factor β was evaluated for all tested specimens to range between 0.18 and 0.67 when they were in DS1 and between 0.20 and 0.87 at the attainment of peak strength (not considering CS-00-RF2 for the reasons highlighted above). An average value of β of 0.44 (C.o.V. of 43%) was calculated for all nine specimens tested (in DS1). In the absence of more detailed calculations, a value of $\beta = 0.5$ is suggested to be used for evaluating the OOP displacements of similar URM walls using Eq. (7), i.e. $\alpha = 0.5 \cdot (\alpha_{SS} - \alpha_{FF}) + \alpha_{FF}$. Both the values of α_{SS} and α_{FF} are to be adopted from Fig. 14 or from [48,49]. Physically, this finding implies that the fully interlocking connections of the OOP panel with the return walls provide a restraint connection which is intermediate between a completely fixed and a simply supported scenario in both an undamaged configuration (DS1) as well until the attainment of peak force resistance Consequently, with a reasonable estimate of E (the modulus of elasticity of masonry in vertical compression), Eq. (7) with input from Fig. 14 can be very easily used to predict the displacement response of URM walls under OOP two-way bending excitation at least until the attainment of the peak strength.

An important assumption made in the theory behind this methodology is that points lying on a normal to the middle plane of the wall before bending continue to lie on the normal to the middle plane of the wall after bending. Such an assumption basically translates to disregarding the effect of shear forces on the bending deflection of the walls. This assumption is however not valid for plates with openings where the effect of shear becomes important [48]. Consequently, the predictions for CSW-000-RF [22] correspond to the CSW-000-RF* configuration (i.e. considers only the longer solid panel on either side of the opening and the vertical edge of the opening to be free) suggested to be considered by the authors in [22] for walls with openings while predicting their peak force resistance. Such an assumption was again observed to give good results when compared to experimental recorded data.

It is important to note here that the calculated value of $\beta \approx 0.5$ is not reasoned as an explanation behind the assumption of 50% of the horizontal bending moment capacity at vertical edges contributing to the peak strength of the wall giving a good fit with experimental results in the current study as well as [22,28], which could presumably also be a result of all cracks not reaching their full capacity simultaneously.

7. Concluding remarks

This paper presents the experimental results of incremental dynamic tests on four full-scale URM walls tested in the OOP direction under two-way bending excitation. These included the first test reported in literature when a full-scale wall was subjected to horizontal (OOP) and vertical dynamic input simultaneously. However, no effect of the vertical excitation was perceived in the OOP response of the “Weak Unit –Strong Joint” (WU-SJ) masonry wall restrained on all three sides and kept free on the top subjected to simultaneous OOP and vertical seismic excitation compared to the wall subjected to just OOP excitation. This is best attributed to the fact that under such boundary conditions, the failure mechanism of the wall is controlled by the splitting of masonry units which is hardly affected by the acting axial load. Additionally, two walls with different aspect ratios were also tested in a boundary condition that has not been assessed experimentally in previous studies: with two adjacent edges restrained and the other two edges free. Similar to the specimens in WU-SJ masonry tested in Graziotti *et al.* [22], all specimens tested in this campaign exhibited a very brittle behaviour and negligible energy dissipation capacity. Such behaviour can be indicative of major differences in the vulnerability of walls constructed in “Weak Unit –Strong Joint” and “Strong Unit – Weak Joint” masonry, something that should be explored with simplified numerical models calibrated with the data generated from both the current study and [22,23], combined with more studies on the post-peak behaviour of these walls.

These specimens tested in this study were constructed in mortar deliberately weakened in comparison to the mortar used in Graziotti *et al.* [22] by the addition of sand while using the same units. This was done in order to change the typology of URM from a WU-SJ configuration to a SU-WJ configuration. Despite using state-of-the-art analytical models in literature, the desired transformation of the typology of masonry was not achieved. However, this exercise allowed the identification of the component of these equations which prevented this change in configuration and needs further investigation: the torsional

shear strength of URM bed-joints. A detailed experimental and numerical investigation into the torsional shear strength of URM bed-joints is hence even more warranted.

The theory of plates was successfully applied to predict the displacement at the attainment of peak strength of all specimens tested in the current study as well as [22]. Charts are provided based on this theory which can be used in practice for estimating the expected displacements of URM walls under restraint conditions and in aspect ratios commonly found in practice. A key observation of all the experiments was the limited post-peak behaviour associated with the tested specimens. Considering this, such formulation combined with a virtual-work-based methodology for estimating peak strength present a simplified framework which can be practically used for the assessment of the OOP response of URM wall panels under two-way bending action. All experimental data reported in this article is freely available upon request from www.eucentre.it/nam-project.

CRediT authorship contribution statement

S. Sharma: Investigation, Formal analysis, Writing - original draft. **U. Tomassetti:** Conceptualization, Investigation, Visualization. **L. Grottoli:** Data curation, Software, Visualization. **F. Graziotti:** Conceptualization, Supervision, Writing - review & editing.

Declaration of competing interest

The authors declare that they have no known competing financial interests or personal relationships that could have appeared to influence the work reported in this paper.

Acknowledgments

This paper describes an activity that is part of the “Study of the vulnerability of masonry buildings in Groningen” project at the EUCENTRE within the framework of the research program for hazard and risk of induced seismicity in Groningen sponsored by the Nederlandse Aardolie Maatschappij (NAM) BV. The authors would like to thank all the parties involved in this project, namely: EUCENTRE, University of Pavia (DICAr), NAM, Arup and TU Delft. The valuable guidance of G. Magenes, A. Penna, R. Pinho, J. Uilenreef, H. Crowley and M. Griffith is gratefully acknowledged. Thanks go also to F. Dacarro, S. Peloso, L. Moriconi, M. P. Scovenna and G. Sinopoli for the practical support.

References

[1] Magenes G, Calvi GM. In-plane seismic response of brick masonry walls. Earthq Eng Struct Dyn 1997;26:1091–112. https://doi.org/10.1002/(SICI)1096-9845(199711)26:11<1091::AID-EQE693>3.0.CO;2-6.
[2] Tomaževič M, Klemenc I. Seismic behaviour of confined masonry walls. Earthq Eng Struct Dyn 1997;26:1059–71. https://doi.org/10.1002/(SICI)1096-9845(199710)26:10<1059::AID-EQE694>3.0.CO;2-M.
[3] Anthoine A, Magonette G, Magenes G. Shear-compression testing and analysis of brick masonry walls. In: Proc 10th Eur Conf Earthq Eng, Vienna, Austria; 1995.
[4] Paquette J, Bruneau M. Pseudo-dynamic testing of unreinforced masonry building with flexible diaphragm. J Struct Eng 2003;129:708–16. https://doi.org/10.1061/(ASCE)0733-9445(2003)129:6(708).
[5] Moon L, Dizhur D, Senaldi I, Derakhshan H, Griffith M, Magenes G, et al. The demise of the URM building stock in Christchurch during the 2010–2011 Canterbury earthquake sequence. Earthq Spectra 2014;30:253–76. https://doi.org/10.1193/022113EQS044M.
[6] Page AW. The Newcastle earthquake – behaviour of masonry structures. Mason Int 1991;5:11–8.
[7] Penna A, Morandi P, Rota M, Manzini CF, da Porto F, Magenes G. Performance of masonry buildings during the Emilia 2012 earthquake. Bull Earthq Eng 2014;12:2255–73. https://doi.org/10.1007/s10518-013-9496-6.
[8] Oyarzo-Vera C, Griffith MC. The Mw 6.3 Abruzzo (Italy) earthquake of April 6th, 2009. Bull New Zeal Soc Earthq Eng 2009. https://doi.org/10.5459/bnzsee.42.4.302-307.
[9] D’Ayala DF, Paganoni S. Assessment and analysis of damage in L’Aquila historic city centre after 6th April 2009. Bull Earthq Eng 2011;9:81–104. https://doi.org/10.1007/s10518-010-9224-4.
[10] Griffith MC, Lam NTK, Wilson JL, Doherty K. Experimental investigation of unreinforced brick masonry walls in flexure. J Struct Eng 2004;130:423–32. https://doi.org/10.1061/(ASCE)0733-9445(2004)130:3(423).
[11] Graziotti F, Tomassetti U, Penna A, Magenes G. Out-of-plane shaking table tests on URM single leaf and cavity walls. Eng Struct 2016;125. https://doi.org/10.1016/j.engstruct.2016.07.011.
[12] Penner O, Elwood KJ. Out-of-plane dynamic stability of unreinforced masonry walls in one-way bending: parametric study and assessment guidelines. Earthq Spectra 2016;32:1699–723. https://doi.org/10.1193/011715EQS011M.
[13] Simsir CC, Aschheim MA, Abrams DP. Out-of-plane dynamic response of unreinforced bearing walls attached to flexible diaphragms. In: Proc 13th World Conf Earthq Eng, Vancouver, British Columbia, Canada; 2004.
[14] Giaretton M, Dizhur D, Ingham JM. Dynamic testing of as-built clay brick unreinforced masonry parapets. Eng Struct 2016;127:676–85. https://doi.org/10.1016/j.engstruct.2016.09.016.
[15] Restrepo-Vélez LF, Magenes G, Griffith MC. Dry stone masonry walls in bending - Part I: Static tests. Int J Archit Herit 2014;8:1–28. https://doi.org/10.1080/15583058.2012.663059.
[16] Vaculik J, Griffith MC, Hogarth B, Todd J. Out-of-plane flexural response tests using dry-stack masonry. In: Proc Aust Earthq Soc Conf, Mt Gambier, South Australia; 2004.
[17] Maccarini H, Vasconcelos G, Rodrigues H, Ortega J, Lourenço PB. Out-of-plane behavior of stone masonry walls: experimental and numerical analysis. Constr Build Mater 2018. https://doi.org/10.1016/j.conbuildmat.2018.05.216.
[18] Griffith MC, Vaculik J, Lam NTK, Wilson J, Lumantarna E. Cyclic testing of unreinforced masonry walls in two-way bending. Earthq Eng Struct Dyn 2007;36:801–21. https://doi.org/10.1002/eqe.654.
[19] Damiola M, Esposito R, Messali F, Rots JG. Quasi-static cyclic two-way out-of-plane bending tests and analytical models comparison for URM walls. In: Proc 10th Int Mason Conf, Milan, Italy; 2018.
[20] Vaculik J, Griffith MC. Out-of-plane shaketable testing of unreinforced masonry walls in two-way bending. Bull Earthq Eng 2018. https://doi.org/10.1007/s10518-017-0282-8.
[21] Walsh KQ, Dizhur D, Shafaei J, Derakhshan H, Ingham JM. In situ out-of-plane testing of unreinforced masonry cavity walls in as-built and improved conditions. Structures 2015;3:187–99. https://doi.org/10.1016/j.istruc.2015.04.005.
[22] Graziotti F, Tomassetti U, Sharma S, Grottoli L, Magenes G. Experimental response of URM single leaf and cavity walls in out-of-plane two-way bending generated by seismic excitation. Constr Build Mater 2019;195:650–70. https://doi.org/10.1016/j.conbuildmat.2018.10.076.
[23] Tomassetti U, Grottoli L, Sharma S, Graziotti F. Dataset from dynamic shake-table testing of five full-scale single leaf and cavity URM walls subjected to out-of-plane two-way bending. Data Br 2019. https://doi.org/10.1016/j.dib.2019.103854.
[24] Graziotti F, Penna A, Magenes G. A comprehensive in situ and laboratory testing programme supporting seismic risk analysis of URM buildings subjected to induced earthquakes. Bull Earthq Eng 2018. https://doi.org/10.1007/s10518-018-0478-6.
[25] Van Elk J, Bourne SJ, Oates SJ, Bommer JJ, Pinho R, Crowley H. A probabilistic model to evaluate options for mitigating induced seismic risk. Earthq Spectra 2019. https://doi.org/10.1193/050918EQS118M.
[26] Crowley H, Pinho R, Cavalieri F. Report on the v6 fragility and consequence models for the Groningen field; 2018.
[27] Tomassetti U, Graziotti F, Penna A, Magenes G. Modelling one-way out-of-plane response of single-leaf and cavity walls. Eng Struct 2018. https://doi.org/10.1016/j.engstruct.2018.04.007.
[28] Griffith MC, Vaculik J. Out-of-plane flexural strength of unreinforced clay brick masonry walls. Mason Soc J 2007;25:53–68.
[29] Willis C. Design of unreinforced masonry walls for out-of-plane loading. University of Adelaide; 2004.
[30] Timoshenko SP, Young DH. Elements of strength of materials. 4th ed. New York: Van Nostrand; 1962.
[31] RILEM TC. LUM A2 Flexural strength of masonry units, 1991. RILEM Recomm. Test. Use Constr. Mater., E & FN SPON; 1994, p. 459–61.
[32] AS 3700-2001:Masonry Structures, Australian Standard, Sydney, Australia; 2001.
[33] EN 1052-5. Methods of test for masonry – Part 5: Determination of bond strength by the bond wrench method. Brussels, Belgium: European Standards, CEN/TC; 2005.
[34] EN 1052-1. Methods of test for masonry – Part 1: Determination of compressive strength. Brussels, Belgium: European Standards, CEN/TC; 1998.
[35] EN 1015-11. Methods of test for mortar for masonry – Part 11: Determination of flexural and compressive strength of hardened mortar. Brussels, Belgium: European Standards, CEN/TC; 1999.
[36] EN 772-1. Methods of test for masonry units – Part 1: Determination of compressive strength. European Standards, CEN/TC, Brussels, Belgium; 2011.
[37] EN 1052-3. Methods of test for masonry – Part 3: Determination of initial shear strength. Brussels, Belgium: European Standards, CEN/TC; 2002.
[38] EN 1052-2. Methods of test for masonry – Part 2: Determination of flexural strength. Brussels, Belgium: European Standards, CEN/TC; 1999.
[39] Vaculik J, Griffith MC. Probabilistic analysis of unreinforced brick masonry walls subjected to horizontal bending. J Eng Mech 2017;143.. https://doi.org/10.1061/(ASCE)EM.1943-7889.0001266.
[40] Casapulla C, Portioli F. Experimental investigation on the torsion-shear interaction between stone blocks in frictional contact. Struct Stud Repairs Maint Heritage Arch XIV 2015:429–40. https://doi.org/10.2495/STR150361.
[41] Orduña A, Lourenço PB. Three-dimensional limit analysis of rigid blocks assemblages. Part I: Torsion failure on frictional interfaces and limit analysis formulation. Int J Solids Struct 2005. https://doi.org/10.1016/j.ijsolstr.2005.02.010.

[42] Samarasinghe W, Lawrence SJ. Behaviour of masonry under combined torsion and compression. 10th IBMAC, Calgary, Canada; 1994.
[43] Derakhshan H, Lucas W, Visintin P, Griffith MC. Out-of-plane strength of existing two-way spanning solid and cavity unreinforced masonry walls. Structures 2018;13:88–101. https://doi.org/10.1016/j.istruc.2017.11.002.
[44] Graziotti F, Tomassetti U, Kallioras S, Penna A, Magenes G. Shaking table test on a full scale URM cavity wall building. Bull Earthq Eng 2017;15. https://doi.org/10.1007/s10518-017-0185-8.
[45] Bommer JJ, Crowley H, Pinho R, Polidoro B. Selection of acceleration time-series for shake table testing of Groningen masonry building at the Eucentre, Pavia; Report – Groningen field seismic hazard and risk assessment project. Pavia Italy; 2015.
[46] Eucentre. Videos of full-scale shaking table test on a URM cavity-wall building model 2015. https://www.youtube.com/watch?v=h8sZCRUCons&list=PLRDMVFxhFvQm8pxSTPpzHN1AQH0G7sMGk.%0A.
[47] Tomassetti U, Correia AA, Candeias PX, Graziotti F, Campos Costa A. Two-way bending out-of-plane collapse of a full-scale URM building tested on a shake table. Bull Earthq Eng 2019;17:2165–98. https://doi.org/10.1007/s10518-018-0507-5.
[48] Timoshenko S, Woinowsky-Krieger S. Theory of plates and shells. 2nd ed. New York: McGRAW HILL BOOK COMPANY; 1940.
[49] Liu Y, Li R. Accurate bending analysis of rectangular plates with two adjacent edges free and the others clamped or simply supported based on new symplectic approach. Appl Math Model 2010;34:856–65. https://doi.org/10.1016/j.apm.2009.07.003.